

# SCN as a Local Probe of Protein Structural Dynamics

Sena Aydin,<sup>†,¶</sup> Seyedeh Maryam Salehi,<sup>†,¶</sup> Kai Töpfer,<sup>†</sup> and Markus Meuwly<sup>\*,†,‡</sup>

<sup>†</sup>*Department of Chemistry, University of Basel, Klingelbergstrasse 80, CH-4056 Basel, Switzerland.*

<sup>‡</sup>*Department of Chemistry, Brown University, RI 02912, USA*

<sup>¶</sup>*These authors contributed equally*

E-mail: m.meuwly@unibas.ch

April 30, 2024

## Abstract

The dynamics of lysozyme is probed by attaching -SCN to all alanine-residues. The 1-dimensional infrared spectra exhibit frequency shifts in the position of the maximum absorption by  $4\text{ cm}^{-1}$  which is consistent with experiments in different solvents and indicates moderately strong interactions of the vibrational probe with its environment. Isotopic substitution  $^{12}\text{C} \rightarrow ^{13}\text{C}$  leads to a red-shift by  $-47\text{ cm}^{-1}$  which is consistent with experiments with results on CN-substituted copper complexes in solution. The low-frequency, far-infrared part of the protein spectra contain label-specific information in the difference spectra when compared with the wild type protein. Depending on the positioning of the labels, local structural changes are observed. For example, introducing the -SCN label at Ala129 leads to breaking of the  $\alpha$ -helical structure with concomitant change in the far-infrared spectrum. Finally, changes in the local hydration of SCN-labelled Alanine residues as a function of time can be related to angular reorientation of

the label. It is concluded that -SCN is potentially useful for probing protein dynamics, both in the high-frequency (CN-stretch) and far-infrared part of the spectrum.

## 1 Introduction

Characterizing the dynamics of proteins in solution is essential for understanding their function and interactions with their environment which is particularly relevant in a physiological and cellular context.<sup>1</sup> Because functional motions of proteins can involve local and/or more global changes in their structure and single protein structures are not sufficient to explain a protein's function,<sup>2</sup> it is of particular interest to delineate protein structural changes on given time scales. One technique to link structure, dynamics and the time scales on which they develop is optical spectroscopy, in particular infrared (IR) spectroscopy.<sup>3-7</sup> Recent progress in synchronization of femtosecond laser pulses allowed to map out the entire reaction cycle of bacteriorhodopsin.<sup>8</sup>

To gain site-specific information on local protein dynamics, significant effort has been focused on developing chemical groups suitable for frequency-resolved spectroscopy.<sup>9-11</sup> For instance, -CD bonds have been shown to be suitable to map out the local dynamics within a protein.<sup>12</sup> In another work, attaching a ruthenium carbonyl complex to the His15 residue in both hen egg white and human lysozyme, allowed to investigate the local hydration of the proteins via IR spectroscopy.<sup>13</sup> Finally, <sup>13</sup>C as a site-specific isotopic label was introduced to examine the secondary structures of the residues in conformationally heterogeneous peptides.<sup>14</sup> Using computer simulations it has been shown that AlaN<sub>3</sub> is a position-sensitive probe, providing useful information on the protein modification site in previous work.<sup>15</sup>

Cyanide (-CN) and thiocyanate (-SCN) are nitrile-based vibrational probes that can be integrated into proteins and have been used, for example, to label alanine residues.<sup>16-18</sup> When

the -SCN moiety is incorporated into peptides or proteins, it gives rise to absorption bands owing to its comparatively large extinction coefficient between 100 to 300  $\text{M}^{-1}\text{cm}^{-1}$ .<sup>19,20</sup> The IR stretching absorption values of SCN-labelled proteins change between 2151 and 2161  $\text{cm}^{-1}$  and it is sensitive to its environment acting as a site-specific electric field probe for proteins.<sup>19</sup> The -SCN probe has also been attached to alanine to form  $\beta$ -thiocyanatoalanine for which NMR<sup>21,22</sup> and IR studies in solution had been carried out. Moreover, the lifetime of the C-N stretching mode in a -SCN label is sensitive to the surrounding environment, owing to the decoupling of the CN-label and the rest of the amino acid due to the sulfur atom, which has been referred to as the “insulating effect”.<sup>11,23</sup> Similar results were observed in a study of methyl thiocyanate (MeSCN) in different solvents.<sup>24</sup>

In the present work, -SCN is used as a spectroscopic probe to elucidate local protein dynamics. The label is attached to all 16 alanine residues of the lysozyme protein to investigate the differences in the local and global dynamics of the protein. First, the methods are described, followed by a validation of the potential energy surfaces (PES). Next, the protein IR spectroscopy and the dynamics of the spectroscopic probe is described for lysozyme with all alanine-residues labelled with -SCN. Finally, the results are discussed and conclusions are drawn.

## 2 Methods

### 2.1 The Potential Energy Surface

The energy function is integrated with CHARMM<sup>25</sup> force field and the regenerating kernel Hilbert space (RKHS)<sup>26,27</sup> PES to probe spectroscopic methods for the protein structure. Starting from an optimized structure of thiocyanatoalanine at the MP2/aug-cc-pVTZ level of theory, the PES for the -SCN label is calculated using pair natural orbital-based coupled

cluster level (PNO-LCCSD(T)-F12)<sup>28,29</sup> together with the aug-cc-pVTZ basis set<sup>30</sup> using MOLPRO software.<sup>31</sup> The *ab initio* energies were calculated in Jacobi coordinates  $(R, r, \theta)$ , where  $r$  is the distance between carbon and nitrogen atoms,  $R$  is the distance between their center of mass and sulfur atom, and  $\theta$  is the angle between  $\vec{r}$  and  $\vec{R}$ , see the inset of Figure 1. The angular grid ( $\theta$ ) used here contains 6 points between 150 to 180° while radial grids include 16 points along  $r$  ranging from 0.92 to 1.68 Å and 13 points along  $R$  between 1.82 and 2.82 Å. A dihedral angle  $\phi$  is defined between the planes spanned by  $\vec{r}$  and  $\vec{R}$  of the -SCN label and the vector from the anchor carbon atom of alanine and the sulfur atom of the -SCN label with  $\vec{R}$ . That dihedral angle  $\phi$  is preserved for the energy calculations as in the equilibrium conformation  $\phi_{\text{eq}} = 11.3^\circ$ . The equilibrium Jacobi angle  $\theta$  is  $\sim 180^\circ$ .

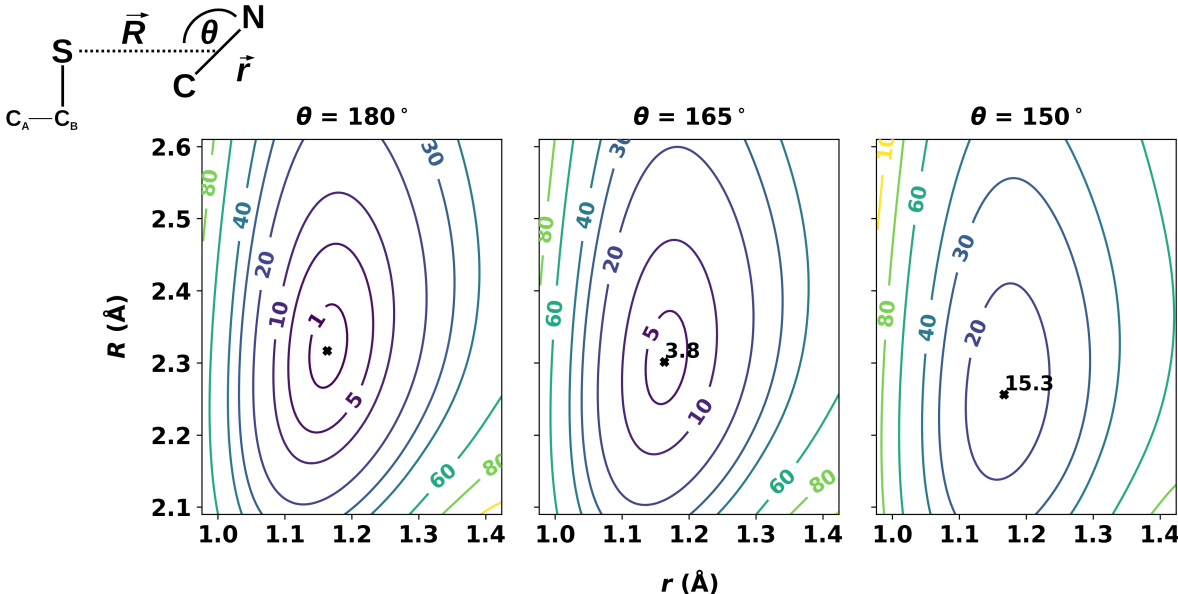


Figure 1: Contour representation of the RKHS PES for -SCN label based on PNO-LCCSD(T)-F12 *ab initio* points in Jacobi coordinates  $(R, r, \theta)$  for  $\theta = 180.0^\circ$ ,  $\theta = 165.0^\circ$ , and  $\theta = 150.0^\circ$ , from left to right. The black cross in the center of each panel shows the minima of the PES at the fixed angle in kcal/mol (for  $\theta = 180.0^\circ$  it is 0 kcal/mol). The schematic representation of -SCN Jacobi coordinates are given in the left corner of the figure.

For the differentiable representation of the *ab initio* energies using the RKHS approach<sup>26,27</sup>

only coupled cluster results with a T1 diagnostic value<sup>32</sup> lower than 0.02 are used. The condition excludes, among others, all reference points with  $r > 1.4 \text{ \AA}$  for the construction of the RKHS potential. Still, the included reference points cover the conformation space with respective potential energies up to 70 kcal/mol around the minimum conformation. Figure 1 demonstrates the RKHS representation of the PES constructed from 842 of the 1248 *ab initio* energies. Note that the PES at  $r > 1.4 \text{ \AA}$  is physically not meaningful due to the exclusion conditions.

## 2.2 Molecular Dynamics Simulations

Molecular Dynamics (MD) simulations for the wild type (WT) and all modified AlaQQSCN with QQ = 41, 42, 49, 63, 73, 74, 82, 93, 97, 98, 112, 129, 130, 134, 146, and 160 were performed using the CHARMM<sup>33</sup> package starting from the X-ray structure 1L83.<sup>34</sup> To carry out the simulation with the RKHS PES for the spectroscopic label, an interface is written.<sup>35</sup> For the -SCN label a point charge representation based on a natural bond orbital (NBO) analysis of the minimized MP2/aug-cc-pVTZ structure of thiocyanatoalanine was used. The total charge of the -SCN label from this analysis was close to 0 with rescaled partial charges  $q_S = 0.11e$ ,  $q_C = 0.02e$ ,  $q_N = -0.13e$ . The scaling was determined from comparing the NBO charges for the alanine residue with those from the CGenFF parametrization. The geometry of the label was defined by a bond between the sulfur atom and the side chain methyl-carbon atom  $C_B$  of alanine, the corresponding  $CSC_B$  angle, and the  $SC_B C_A$  angle but without including the  $NCSC_B$  dihedral angle, see below.

The simulations were carried out in a cubic box of size  $(78)^3 \text{ \AA}^3$  with explicit TIP3P water model. Using the SHAKE<sup>36</sup> algorithm, bond lengths involving H-atoms were constrained. A cutoff of  $14 \text{ \AA}$  with switching at  $10 \text{ \AA}$  was used for non-bonded interactions.<sup>37</sup> In Figure 2, the structure of lysozyme with 16 labelled alanine residues is illustrated. The -SCN label

is attached to each of the 16 alanine residues. For all 16 AlaQQSCN modifications, 2 ns production run was performed in the *NVT* ensemble after the initial minimization, heating, and equilibration.

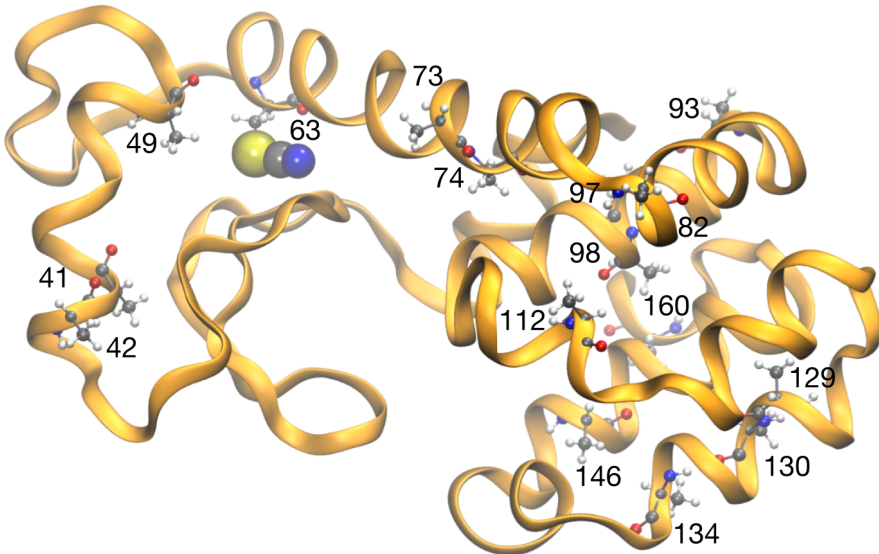


Figure 2: Structure of lysozyme emphasizing the positions of 16 labelled alanine residues. The labelled alanine residues are located at 41, 42, 49, 63, 73, 74, 82, 93, 97, 98, 112, 129, 130, 134, 146, and 160. SCN-labelled Ala63 is shown as an example.

### 2.3 Spectroscopic Analysis

For the protein and subsystems 1-dimensional IR spectra  $I(\omega)$  were obtained from the Fourier transform of the dipole-dipole correlation function

$$I(\omega)n(\omega) \propto Q(\omega) \cdot \text{Im} \int_0^\infty dt e^{i\omega t} \sum_{i=x,y,z} \langle \boldsymbol{\mu}_i(t) \cdot \boldsymbol{\mu}_i(0) \rangle \quad (1)$$

where  $\boldsymbol{\mu}_i(t)$  is the dipole moment vector of the full protein, the modified alanine residue, or the -SCN label. A quantum correction factor  $Q(\omega) = \tanh(\beta\hbar\omega/2)$  was applied to the results of the Fourier transform.<sup>38</sup> This procedure yields lineshapes but not absolute intensities.

As a proxy of the 2-dimensional spectroscopy the frequency fluctuation correlation function (FFCF) was determined. For this, the frequency trajectory  $\omega(t)$  follows the temporal change of the instantaneous CN-normal mode of all 16 AlaQQSCN was calculated for  $4 \times 10^5$  snapshots of each production simulation using instantaneous normal mode (INM) analysis.<sup>39</sup> For each snapshot, the structure of the -SCN label was minimized with frozen environment. From the frequency trajectory  $\omega(t)$  the FFCF of  $\delta\omega(t) = \omega(t) - \langle \omega \rangle$  was determined which contains valuable information on relaxation time scales corresponding to the solvent dynamics around the solute. The FFCFs are fit to an empirical expression

$$\langle \delta\omega(t)\delta\omega(0) \rangle = a_1 \cos(\gamma t)e^{-t/\tau_1} + a_2 e^{-t/\tau_2} + \Delta_0^2 \quad (2)$$

which allows analytical integration to obtain the lineshape function<sup>40</sup> using an automated curve fitting tool from the SciPy library.<sup>41</sup> Here,  $a_i$ ,  $\tau_i$ ,  $\gamma$  and  $\Delta_0^2$  are the amplitudes, decay time scales, phase and asymptotic value of the FFCF. The first time is included in order to model early-time undulations in the FFCF which have been interpreted as solvent-solute interactions.<sup>40,42-44</sup>

## 2.4 Local Hydrophobicity

Calculating the local hydrophobicity (LH) which is defined as a time dependent quantity,  $\delta\lambda_{\text{phob}}^{(r)}(t)$ , is an efficient way to quantify the solvent exposure of amino acids.<sup>45,46</sup> The method analyzes the occupation and orientational statistics of surface water molecules at the protein/water interface using the vector  $\vec{\kappa} = (a, \cos \theta_{\text{OH1}}, \cos \theta_{\text{OH2}})$ . Here,  $a$  is the distance between the nearest atom of residues with oxygen of water molecules, and  $\theta_{\text{OH1}}$  and  $\theta_{\text{OH2}}$  are the angles between the water OH1 and OH2 bonds and the interface normal.<sup>47</sup> Defining the

local hydrophobicity (LH) as  $\delta\lambda_{\text{phob}}^{(r)}(t) = \lambda_{\text{phob}}^{(r)}(t) - \langle\lambda_{\text{phob}}\rangle_0$ , then

$$\lambda_{\text{phob}}^{(r)}(t) = -\frac{1}{\sum_{a=1}^{N_a(r)} N_w(t;a)} \sum_{a=1}^{N_a(r)} \sum_{i=1}^{N_w(t;a)} \ln \left[ \frac{P(\vec{\kappa}^{(i)}(t)|\text{phob})}{P(\vec{\kappa}^{(i)}(t)|\text{bulk})} \right] \quad (3)$$

and  $\langle\lambda_{\text{phob}}\rangle_0$  is the ensemble average for the ideal hydrophobic reference system.  $N_a(r)$  refers to all atoms in residue  $r$  while  $N_w(t;a)$  stands for all water molecules within a cut-off of 6 Å of atom  $a$  at time  $t$ .<sup>47</sup> The vector  $\vec{\kappa}^{(i)}(t)$  defines the  $i$ th water molecule in the sampled population.

The  $P(\vec{\kappa}^{(i)}(t)|\text{phob})$  distribution is based on hydrophobic reference system while  $P(\vec{\kappa}^{(i)}(t)|\text{bulk})$  is obtained from the actual simulation.<sup>45</sup> From this perspective the local hydrophobicity determines the similarity of the water ordering between an ideal hydrophobic system and the one from the simulation. The more dissimilar the two distributions are, the more hydrophilic the environment of the site is and vice versa. Therefore,  $\delta\lambda_{\text{phob}}^{(r)}(t) \approx 0$  indicates a hydrophobic environment around residue  $r$  while  $\delta\lambda_{\text{phob}}^{(r)} > 0.5$  points to a more hydrophilic environment. However, the cutoff magnitude may change depending on the system.<sup>45-47</sup>

## 3 Results

### 3.1 Validation of the PES

The 3-dimensional RKHS representation  $V(R, r, \theta)$  of the -SCN label as a function of the Jacobi coordinates  $\{R, r, \theta\}$  reproduces the reference calculations at the PNO-LCCSD(T)-F12/aug-cc-pVTZ level of theory with an RMSD of  $\sim 0.4$  kcal/mol ( $R^2 = 0.999$ ), see Figure 3A. The geometry was that of the minimum energy structure for thiocyanatoalanine for which all internal coordinates were frozen except for the Jacobi coordinates describing the geometry of the -SCN label. The energies cover a range within 70 kcal/mol of the global minimum. To further validate the quality of the PES, an additional 200 *ab initio* energies were determined



for off-grid geometries for given  $C_A$ SCN dihedral angle  $\phi$ , see Figure 3 for the definition of  $\phi$ . Geometries with  $\{R, r, \theta\}$  are randomly chosen by normal distribution around  $\{2.323 \text{ \AA}, 1.178 \text{ \AA}, 180^\circ\}$  with a standard deviation of  $\{0.15 \text{ \AA}, 0.1 \text{ \AA}, 10.0^\circ\}$  and the dihedral angle was uniformly sampled in the interval  $[0, 360]^\circ$ . Figure 1B confirms the quality of the RKHS-PES with  $\text{RMSD} = 0.652 \text{ kcal/mol}$  and  $R^2 = 0.998$ .

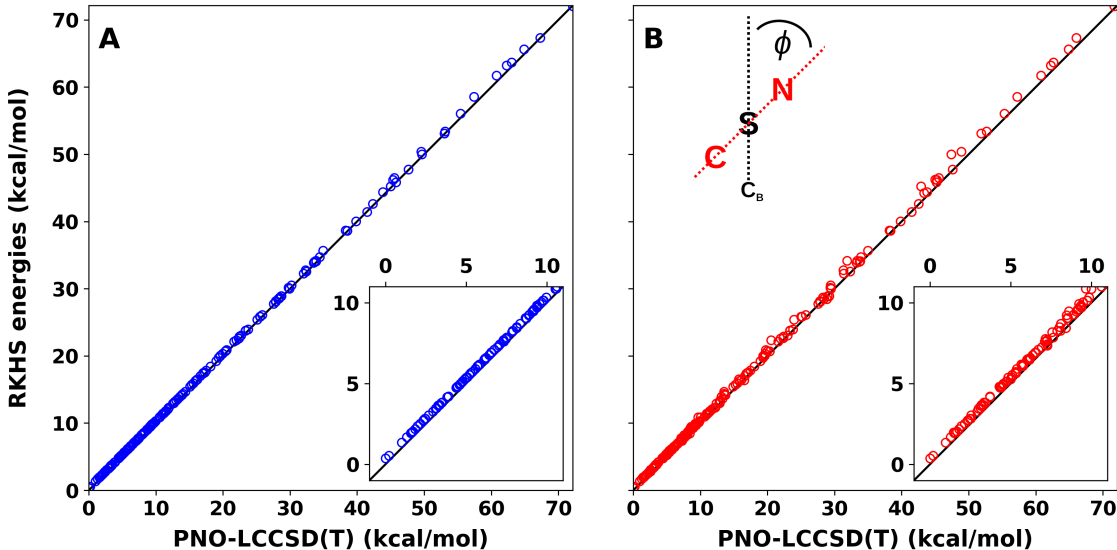


Figure 3: Correlation between PNO-LCCSD(T)/aug-cc-pVTZ reference *ab initio* energies and the RKHS-representation. Panel A: On-grid data for the dihedral fixed at the minimum energy structure ( $\phi = 11.3^\circ$ ) and panel B: for a randomly oriented label with  $\phi \in [0, 360]^\circ$ . For panel A:  $R^2 = 0.999$  and  $\text{RMSD} = 0.384 \text{ kcal/mol}$  and for panel B:  $R^2 = 0.998$  and  $\text{RMSD} = 0.652 \text{ kcal/mol}$ .

### 3.2 Protein and Sub-System Infrared Spectroscopy

First, the 1-dimensional IR spectra of the protein, the modified Ala-residues, and the label were analyzed from the Fourier transform of the dipole-dipole correlation function, see Figure 4 for labelled Ala93. The label-specific, Ala93SCN, and full protein spectra are reported in panels A to C and the vertical dashed lines indicate the bend, symmetric stretch, and asymmetric stretch vibration of -SCN as assigned from the figure.

Figure 4A shows the label-specific IR spectrum determined from the sub-system dipole moment of the -SCN label. Besides the clearly visible internal vibrational modes (bend, symmetric stretch, and asymmetric stretch) additional bands in particular towards lower frequencies arise. Shifted to lower frequencies, additional spectral features arise which represent coupling between the motion of the label and the protein and solvent environment. For Ala93SCN, the peaks are at 2217, 414, and 690  $\text{cm}^{-1}$ .

The IR spectrum of the Ala93SCN subsystem is reported in Figure 4B. The SCN-asymmetric stretch vibration is well removed from the amide, fingerprint and low-frequency vibrations and clearly visible whereas the symmetric stretch disappears entirely. On the other hand, the bending vibration is still visible. This partial IR spectrum also clarifies that the low-frequency modes to which -SCN and Ala93 couple are comparable. In the frequency range above 1000  $\text{cm}^{-1}$  a series of distinct vibrational peaks arises which could be assigned if needed.

Entire proteins have a yet larger density of states and discerning particular features in the vibrational spectroscopy below 2000  $\text{cm}^{-1}$  becomes very challenging, see Figure 4C. A significant increase in the number of vibrational modes is found and only the -SCN asymmetric stretch can still be distinguished. Due to the coupling between the various degrees of freedom many peaks wash out and broaden considerably. However, the overlap for the low-frequency modes (below 250  $\text{cm}^{-1}$ ) in the three spectra is notable.

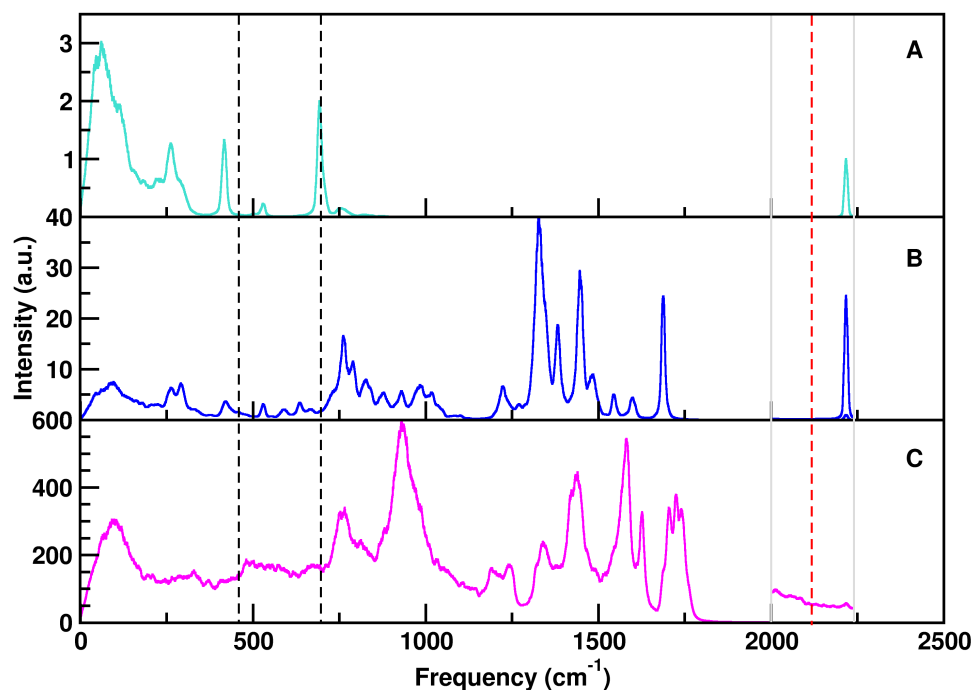


Figure 4: IR spectra of -SCN label (A), labelled Ala93 (B), and full lysozyme (C) for Ala93SCN in lysozyme. The dashed vertical lines denote the specific peaks of -SCN label MeSCN at 459, 697, and 2118  $\text{cm}^{-1}$ . The range highlighted with grey lines between 2000 and 2240  $\text{cm}^{-1}$  is rescaled. The fundamental frequencies of Ala93SCN are at 414, 690, and 2217  $\text{cm}^{-1}$ .

Substituting natural carbon with the  $^{13}\text{C}$  isotope to give a  $-\text{S}^{13}\text{CN}$  label, allows one to probe isotope effect on the IR spectrum which was done for Ala93 $\text{S}^{13}\text{CN}$  in lysozyme. In Figure S2, -SCN and  $-\text{S}^{13}\text{CN}$  label-specific IR spectra (A), IR spectra of Ala93SCN and Ala93 $\text{S}^{13}\text{CN}$  residue (B), and full lysozyme with natural and isotopically substituted  $-\text{S}^{13}\text{CN}$  (C) are reported. The orange dashed line represents IR spectra containing isotopically  $-\text{S}^{13}\text{CN}$  label. In Figure S2A, -SCN and isotope-substituted  $-\text{S}^{13}\text{CN}$  label-specific IR spectra are depicted for the Ala93SCN. Upon comparison, it is noticeable that the CN-stretching frequency shifts to the red by  $-47 \text{ cm}^{-1}$  for the heavier  $-\text{S}^{13}\text{CN}$  labelled Ala93 residue, consistent with related findings for -CN labelled metal complexes in aqueous solution, such as  $\text{Cu}^{13}\text{CN}$ , for which the

red shift was  $-42\text{ cm}^{-1}$ .<sup>48</sup> While the other fundamental peaks of Ala93SCN are 414 and  $690\text{ cm}^{-1}$ , those of the  $\text{S}^{13}\text{CN}$ -attached are 406 and  $687\text{ cm}^{-1}$ , respectively. The isotope effect observed for these peaks is less pronounced than the shift in the C-N stretching vibrational mode.

Next, the -SCN, modified AlaQQSCN, and full protein IR spectra were determined for all 15 remaining SCN-labelled alanine residues, see Figure S1. The -SCN fundamental peaks vary within the ranges of  $2216\text{--}2220\text{ cm}^{-1}$  for  $\nu_1$ ,  $413\text{--}425\text{ cm}^{-1}$  for  $\nu_2$ , and  $686\text{--}713\text{ cm}^{-1}$  for  $\nu_3$ . However, when comparing the AlaQQSCN subsystem and full protein spectra, they also differ depending on the position at which the Ala-residue is located along the polypeptide chain. Hence, IR spectra of each locally labelled alanine residue may have unique fingerprints for lysozyme.

To further investigate this, the IR spectrum for unlabelled (WT) lysozyme was also determined, see black trace in Figure S3. Overall, the spectrum for the WT follows that of all modified proteins. The maximum amplitude in the low-frequency region (below  $\sim 250\text{ cm}^{-1}$ ) is found for the Ala134SCN variant and Ala146SCN has the lowest amplitude in this frequency interval. Analysis of the low-frequency spectra for full lysozyme (Figure 5A) and the label-specific spectra (Figure 5B) for all AlaQQSCN residues confirm that the low-frequency part of the IR spectrum contains label-specific signatures. In Figure 5C, the difference far-infrared spectra between the unmodified and the SCN-labelled proteins for eight alanine residues from Figure 5A are reported. Such difference spectra change depending on the position of the SCN-labelled alanine residue along the polypeptide chain. This may provide further information on the local dynamics.

It is interesting to note that the low-frequency part of the IR spectrum was found to be sensitive to the helical content of proteins.<sup>49</sup> Towards the red part of the maximum at  $100\text{ cm}^{-1}$

the measured spectra superimpose whereas towards the blue part at  $150\text{ cm}^{-1}$  the intensity of lysozyme ( $\alpha$ -helical content of 48 %) is twice that of concanavalin (2 %).<sup>49</sup> Hence, it is of interest to consider changes in this frequency range upon SCN-labelling the alanine residues. Similarly, far-infrared spectroscopy of peptides, lysozyme, and other globular proteins established a pronounced peak between  $100$  and  $200\text{ cm}^{-1}$  depending on the protein considered.<sup>49–52</sup>

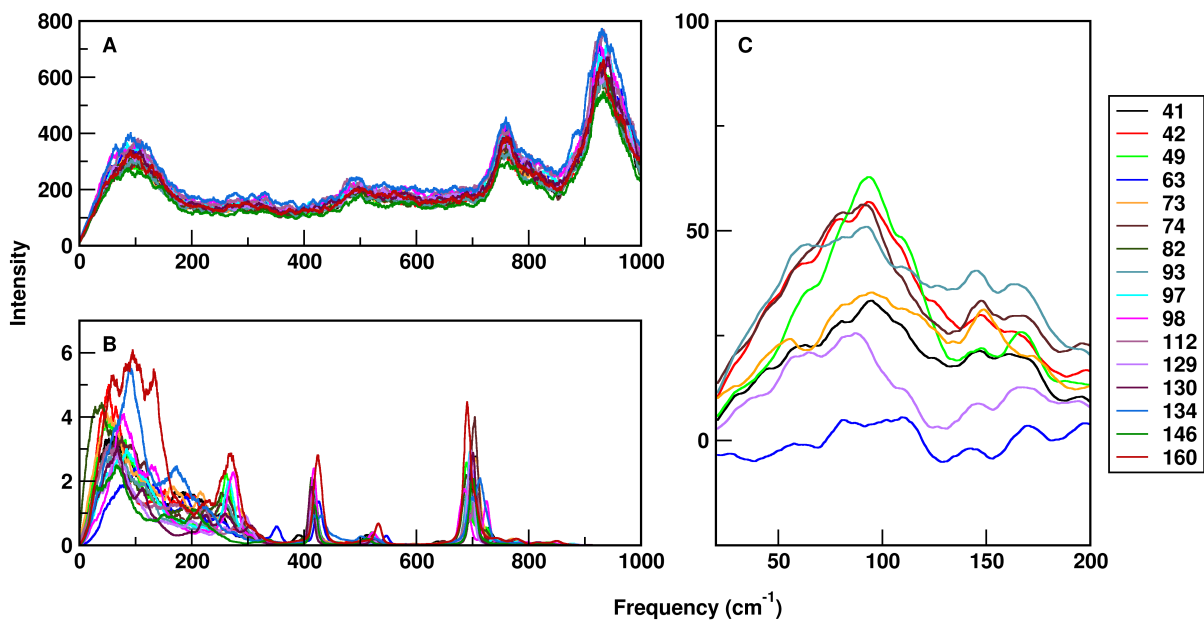


Figure 5: Panel A: IR spectra from the total protein dipole moment time series; panel B: label-specific IR spectra for all 16 AlaQQSCN residues in lysozyme; panel C: the difference IR spectra for the entire protein between WT lysozyme and eight selected AlaQQSCN-labelled lysozyme variants in the far-infrared part of the spectrum. The difference spectrum for Ala129SCN is discussed in the text.

To link protein structural modifications and changes in the (far-)infrared spectroscopy, the case of Ala129SCN was considered specifically. The difference far-infrared spectrum is the violet line in Figure 5C. For the unmodified protein, the secondary structure analysis tool of VMD<sup>53</sup> identifies, among others, three helices extending across residues 126–134, 137–141, and 143–155. Helices 126–134 and 143–155 are positioned in a parallel fashion. For the

modified Ala129SCN protein it is found that on the 2 ns time scale residues 135–142 are in a loop region. In other words, introducing the -SCN label at position 129 partially destroys the helical structure in this region of the protein. This is confirmed by considering the distance between the  $C_\alpha$  atoms of residues Ala129 and Arg154 which increases from  $\sim 7.7$  Å to  $\sim 9.3$  Å after introducing the -SCN label. The difference spectrum between WT and the Ala129SCN-labelled variant (violet line in Figure 5C) features maxima at 88 and 166  $\text{cm}^{-1}$ .

### 3.3 Dynamics of the Spectroscopic Probe

Next, the local dynamics and spectroscopy of the CN-stretch for all modified AlaQQSCN residues were considered. For this, the FFCFs were determined for all 16 modified lysozyme variants using INM calculations. The 1-dimensional IR spectra in the region of the -CN stretch for each -SCN label, see Figure 6, can be calculated from the FFCF. The center frequencies cover a range of  $\sim 4$   $\text{cm}^{-1}$ , extending from 2208  $\text{cm}^{-1}$  for Ala42N<sub>3</sub> to 2212  $\text{cm}^{-1}$  for Ala63N<sub>3</sub> and the full width at half maximum ranges from 13 to 16  $\text{cm}^{-1}$ . This is consistent with the analysis based on the dipole-dipole correlation function (see above) for which the center frequencies cover the range 2216 to 2220  $\text{cm}^{-1}$ , slightly shifted to the blue by  $\sim 10$   $\text{cm}^{-1}$ .

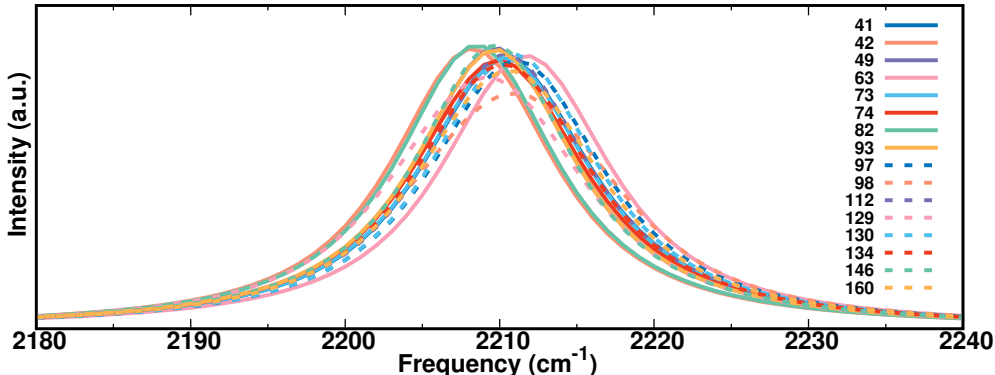


Figure 6: 1D IR spectra obtained from INM analysis for all 16 AlaQQSCN residues in Lysozyme.

Next, the FFCFs themselves are considered, see Figure 7 and Table 1. The majority of FFCFs have a comparatively “simple” behaviour in that they show a rapid initial decay on the sub-ps time scale, followed by a more or less extended decay towards zero on the 5 to 10 ps time scale. Modification sites which differ from this are Ala63SCN, Ala134SCN, and Ala146SCN which show a more pronounced rebound during the first picosecond. As can be seen from Figure 7, residues Ala82SCN, Ala98SCN and Ala129SCN exhibit a considerably slower decay  $\tau_2$ , which may be attributed to the environmentally crowded positioning of the residues. For example, Ala98SCN is located within the interior of the  $\alpha$ -helix, with another helical structure present nearby on the residue’s vicinity. Ala129SCN is positioned in the middle of the  $\alpha$ -helix and, in addition, different  $\alpha$ -helices are located on both sides of it. Ala130SCN and Ala134SCN are also located within the same helical structure as Ala129SCN, but they are positioned further away from the crowded side of the  $\alpha$ -helix compared to Ala129SCN. Therefore, the decay times are faster ( $\sim 23.3$  ps compared with 4.5 and 6.9 ps, respectively). The two decay times are on the sub-ps ( $\tau_1 \leq 0.07$  ps) and several picosecond time scales  $1.47 \leq \tau_2 \leq 23.30$  ps and the amplitude of the fast process is invariably larger than that of the slow process.

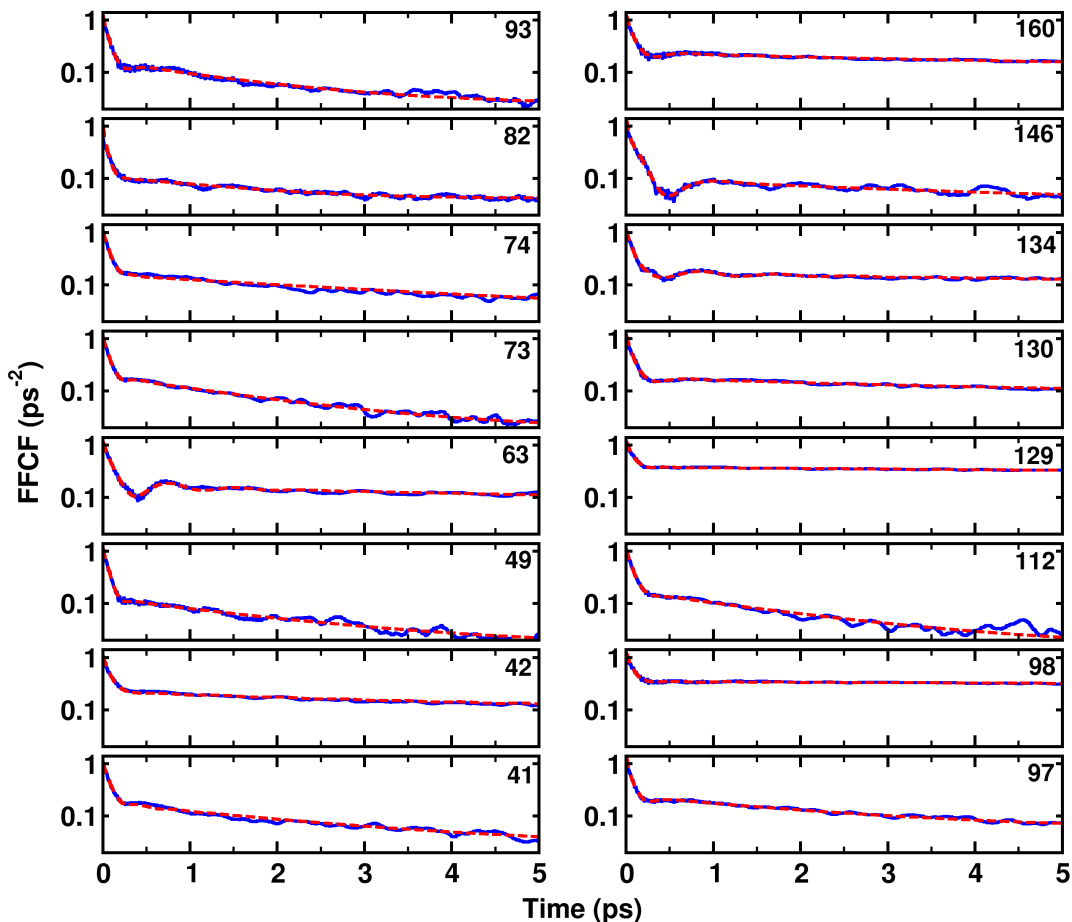


Figure 7: FFCFs obtained using INM analysis for all 16 AlaQQSCN. The labels in each panel refer to the alanine residue which carries the -SCN probe. Blue traces are the raw data and red dashed lines show the fits to Eq. 2. The  $y$ -axis is logarithmic.

The minimum in the FFCF at early correlation times has been observed in experiments<sup>54</sup> and from simulations<sup>15,40,42,43</sup> and has been related to the strength of the intermolecular interaction between the IR probe and its environment.<sup>40,43</sup> Such minima were found for residues Ala63SCN, Ala134SCN, and Ala146SCN. However, they are considerably less pronounced than those observed for azide labelled (-N<sub>3</sub>) in lysozyme.<sup>15</sup>

Residues Ala98SCN, Ala129SCN, and Ala160SCN feature an asymptotic value  $\Delta_0^2$  (“static component”) larger than  $0.1 \text{ cm}^{-1}$ . Such finite values of  $\Delta_0^2$  have been associated with residual



dynamics which has not decayed on the time scale of the analysis. A value of  $\Delta_0^2 = 0.25$  ps<sup>-2</sup>, i.e.  $\Delta_0^2 = 0.5$  ps<sup>-1</sup> corresponds to  $\sim 2.5$  cm<sup>-1</sup>. This is consistent with experimentally measured static components for a nitrile probe (cyanophenylalanine) in HP35 (2.2 cm<sup>-1</sup>) and in S-peptide (2.4 cm<sup>-1</sup>).<sup>55,56</sup> Furthermore, static inhomogeneous components were observed in the spectral diffusion of azide probes in a peptide bound to a protein.<sup>57</sup> Finally, previous simulations of cyano-substituted phenol in lysozyme reported static components of  $\sim 2$  cm<sup>-1</sup>, comparable with the present findings.<sup>58</sup>

Table 1: Parameters obtained from fitting the normalized FFCF to Eq. 2 for INM frequencies for all different AlaQQSCN residues in lysozyme. Average frequency  $\langle\omega\rangle$  of the asymmetric CN-stretch in cm<sup>-1</sup>, the amplitudes  $a_1$  and  $a_2$  in ps<sup>-2</sup>, the decay times  $\tau_1$  and  $\tau_2$  in ps, the parameter  $\gamma$  in ps<sup>-1</sup> and the offset  $\Delta_0^2$  in ps<sup>-2</sup>.

Res	$\langle\omega\rangle$	$a_1$	$\gamma$	$\tau_1$	$a_2$	$\tau_2$	$\Delta_0^2$
<b>41</b>	2209.39	0.84	14.38	0.07	0.16	2.21	0.024
<b>42</b>	2207.26	0.86	9.13	0.07	0.14	4.67	0.083
<b>49</b>	2208.73	0.89	13.11	0.06	0.11	1.82	0.015
<b>63</b>	2210.69	0.88	8.05	0.07	0.1	8.52	0.042
<b>73</b>	2209.33	0.82	13.29	0.06	0.18	1.58	0.017
<b>74</b>	2208.94	0.86	16.72	0.07	0.14	3.82	0.018
<b>82</b>	2207.51	0.94	0.58	0.04	0.06	20.72	0.000
<b>93</b>	2208.71	0.86	9.35	0.04	0.14	1.47	0.024
<b>97</b>	2210.09	0.81	9.11	0.03	0.19	2.18	0.053
<b>98</b>	2209.91	0.91	10.88	0.06	0.09	15.98	0.256
<b>112</b>	2209.42	0.84	9.08	0.06	0.16	1.72	0.014
<b>129</b>	2208.13	0.75	12.08	0.07	0.25	23.30	0.129
<b>130</b>	2209.93	0.89	7.87	0.05	0.11	4.54	0.077
<b>134</b>	2209.22	0.92	7.19	0.06	0.08	6.91	0.087
<b>146</b>	2208.67	0.93	5.18	0.03	0.07	3.37	0.034
<b>160</b>	2109.58	0.87	8.36	0.05	0.13	4.94	0.111

## 4 Discussion and Conclusion

The present work investigated and quantified changes in spectroscopy and local dynamics for SCN-labelled alanine residues in lysozyme. From two different analyses of the IR spectroscopy in the region of the CN-stretch vibration it was found that the maxima in the 1-dimensional IR spectra cover a range of 4 cm<sup>-1</sup>. The dynamics as inferred from the decay of the FFCF

for the 16 sites is characterized by a first sub-ps decay time and a slower time scale  $\tau_2$  which ranges from 1.5 ps to 23.3 ps. Also, several positions along the polypeptide chain feature a static component  $\Delta_0^2$  different from zero which points towards arrested dynamics on the time scale of the analysis. The label-specific difference spectra between unmodified and modified lysozyme indicate that the low frequency modes respond differentially to the position at which the label is placed.

Other spectroscopic probes have been considered in the past to elucidate protein structural dynamics, including nitrile probes to clarify the role of electrostatic fields in enzymatic reactions<sup>59,60</sup> or to elucidate the mode of drug binding to proteins.<sup>61,62</sup> Other labels include cyanamide,<sup>63</sup> sulfhydryl vibrations of cysteines,<sup>64</sup> deuterated carbons,<sup>65</sup> carbonyl vibrations of metal-carbonyls,<sup>66-68</sup> or cyanophenylalanine.<sup>69</sup> Finally, for azidohomoalanine experiments<sup>70</sup> and simulations<sup>15</sup> have explored its utility as a position-sensitive probe. When attached to lysozyme,  $-\text{N}_3$  was found to cover a frequency range of  $\sim 15 \text{ cm}^{-1}$  compared with a frequency span of  $\sim 10 \text{ cm}^{-1}$  when attached to Val, Ala, or Glu in PDZ2.<sup>70</sup> This compares with  $4 \text{ cm}^{-1}$  in the present case for  $-\text{SCN}$  and may be in part due to using a simpler point charge-based model rather than a more elaborate multipolar model for the electrostatics.<sup>71-74</sup>

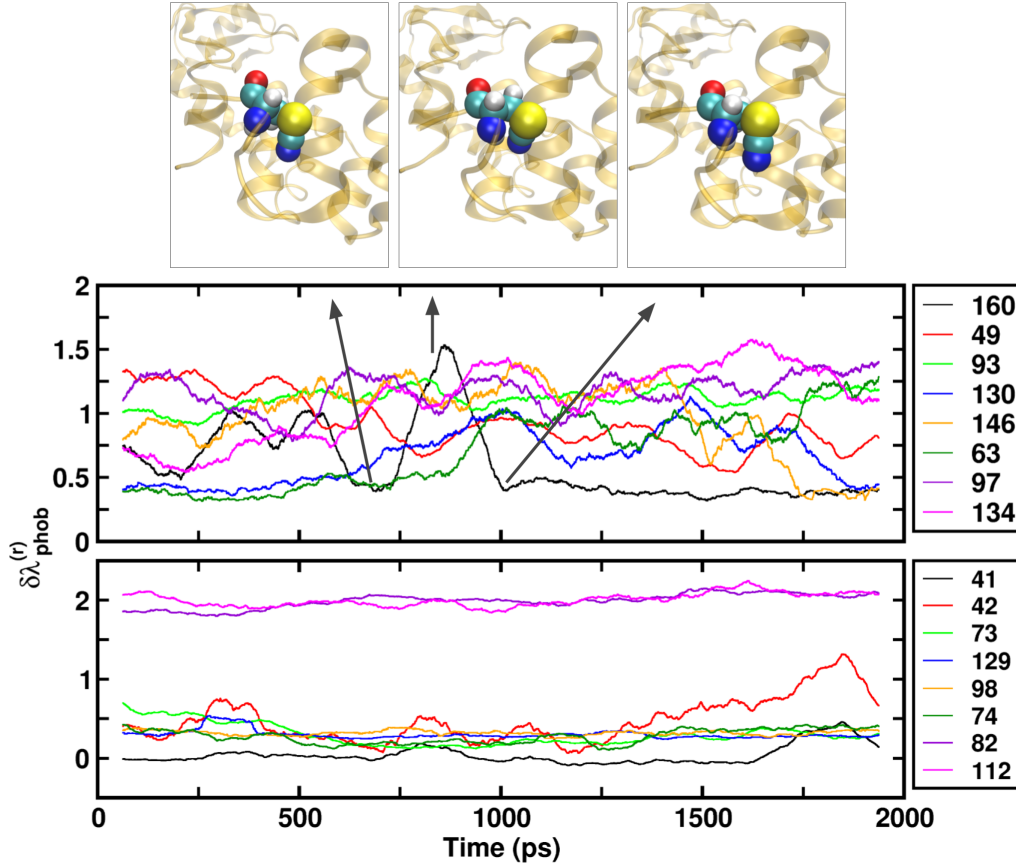


Figure 8: Local hydrophobicity as a function of simulation time for all alanine residues for SCN-labelled lysozyme. The LH coefficient was determined from Eq. 3. Values for  $\delta\lambda_{\text{phob}} \sim 0$  and  $\delta\lambda_{\text{phob}} \sim 2$  are indicative of hydrophobic and hydrophilic environments, respectively.<sup>46,47</sup> The top three panels display various structures from MD simulations of Ala160SCN. These structures depict the temporal structural changes in time and are generated around at 630 ps, 840 ps, and 1 ns, respectively.

The FFCFs of only a few residues show recurrences. These features were found in previous simulations<sup>42,43</sup> and in experiments<sup>54</sup> and have been related to the strength of the intermolecular interaction between the IR probe and its environment.<sup>40,43</sup> Together with the smaller frequency range and frequency shifts of the CN-stretch vibration this indicates that the -SCN label interacts less strongly with its environment. This is consistent with rather narrow frequency shifts for compounds such as MeSCN in polar, non-polar, and protic solvents, covering only  $9 \text{ cm}^{-1}$  for the frequency maximum.<sup>75,76</sup> This compares with  $4 \text{ cm}^{-1}$  from the

present work for -SCN attached to protein-alanine residues in water. The frequency maxima in the present work are around  $2220 \text{ cm}^{-1}$  whereas experimentally this is shifted to the red by  $-60 \text{ cm}^{-1}$ . This is mainly due to the level of theory which was used for constructing the 3-dimensional PES for the -SCN label. It is possible that the frequency spread and position of the frequency maximum shift somewhat more if a more elaborate multipolar or distributed charge model is used.<sup>73,74,77,78</sup> However, given that the -SCN label is electrically close to neutral, i.e.  $\text{SCN}^0$ , such effects are expected to be small.

The frequency shifts observed for the 16 different positions at which the -SCN label was placed is due to both, the exposure of the spectroscopic label to water and the immediate protein environment. One way to analyze the solvent exposure of the labelled alanine-residues is to determine their local hydrophobicity. Figure 8 reports the local hydrophobicity as a function of simulation time for all 16 SCN-labelled alanine residues in lysozyme. suggesting the time-dependence characteristic of LH which is more pronounced for Ala160. On the other hand, without the spectroscopic label, Ala41 with  $\delta\lambda_{\text{phob}}^{(r)}(t) \approx 0$  is clearly hydrophobic while Ala82 and Ala112 with  $\delta\lambda_{\text{phob}}^{(r)}(t) \approx 2$  have high hydrophobicity character. The LH for alanine residues show both low and high values, indicative of hydrophobic and hydrophilic environments, respectively.

To link protein dynamics and local hydrophobicity the case of Ala160SCN is considered (black thick line in Figure 8 top panel). Between 600 ps and 1 ns the value of  $\delta\lambda_{\text{phob}}^{(r)}(t)$  changes from 0.5 to 1.5 and back to 0.5. The corresponding protein structures are shown on top of Figure 8. It is found the local hydrophobicity at position Ala160 can be directly linked to a structural change in that the orientation of the -SCN label changes. This modifies the exposure to solvent water which in turn affects the value of  $\delta\lambda_{\text{phob}}^{(r)}(t)$ . Protein modification has also been found to influence the local dynamics and hydration for S-nitrosylation in myoglobin, hemoglobin, and K-RAS.<sup>79,80</sup>

In summary, the present work characterized the local dynamics around SCN-labelled alanine residues in lysozyme. The IR spectroscopy in the region of the CN-stretch vibration is position-sensitive with maxima in the 1-dimensional lineshape extending across  $4\text{ cm}^{-1}$  which can be detected experimentally and assigned from simulations.<sup>58,81</sup> The IR spectroscopy from the dipole-dipole correlation function and the analysis of the FFCF are consistent with one another and the FFCFs exhibit static components depending on the position of the -SCN label that are supported by earlier experiments and simulations. Finally, the low-frequency spectra, up to  $\sim 300\text{ cm}^{-1}$ , of the labelled proteins differ. This provides a viable route for characterizing different global motions in the modified proteins depending on the modification sites.

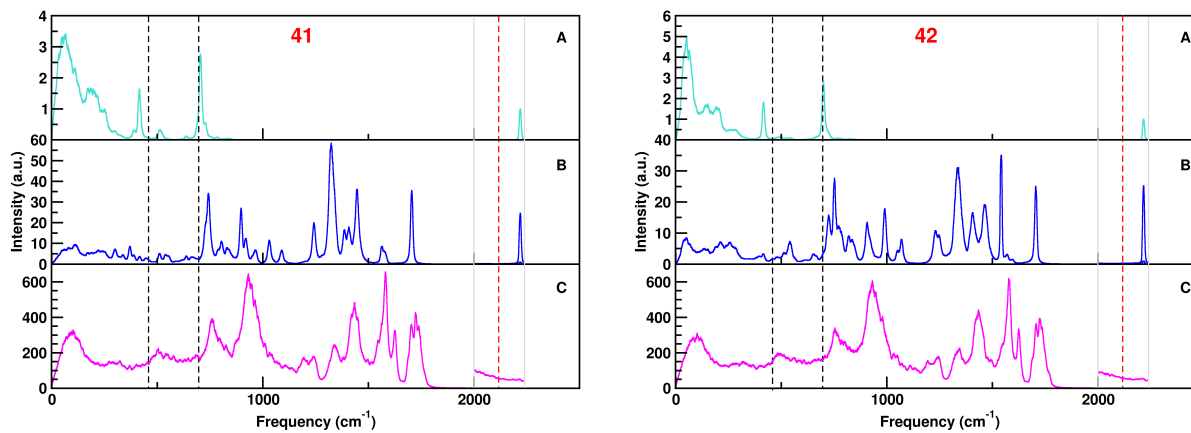
## Acknowledgments

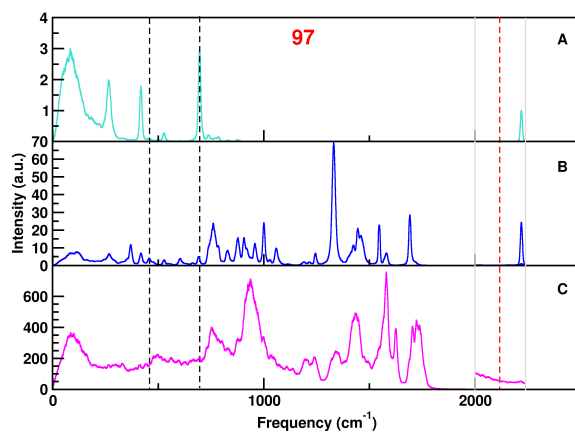
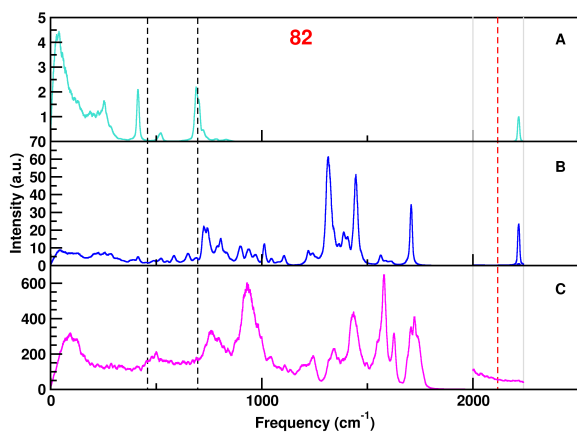
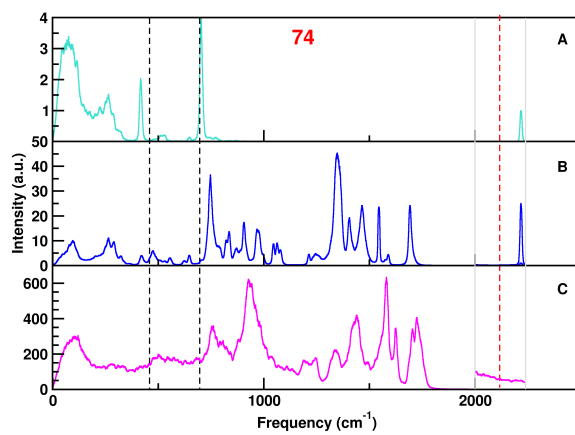
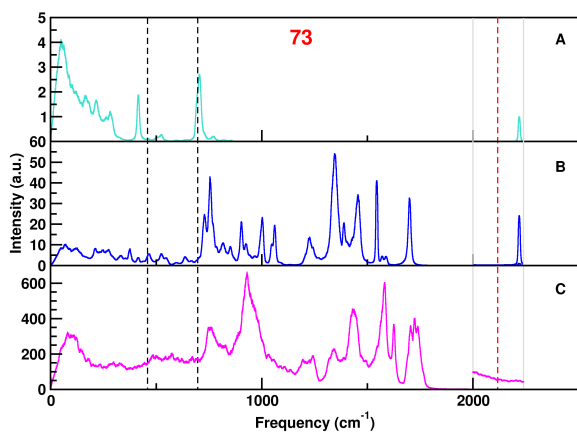
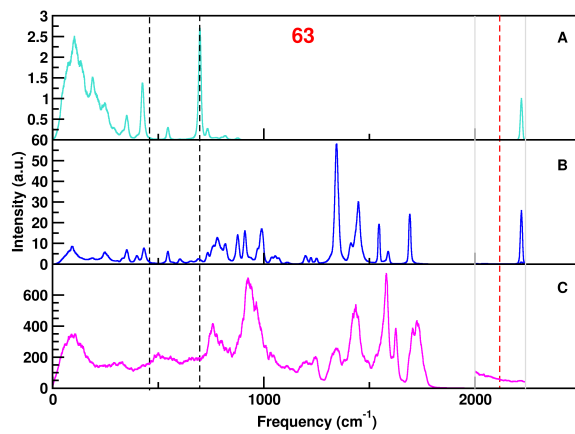
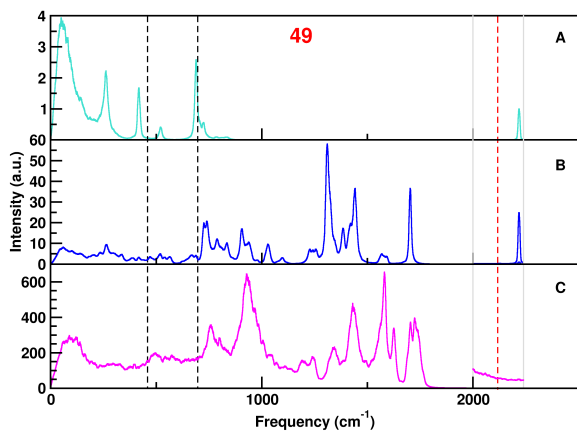
The authors gratefully acknowledge financial support from the Swiss National Science Foundation through grant 200021-117810 and to the NCCR-MUST.

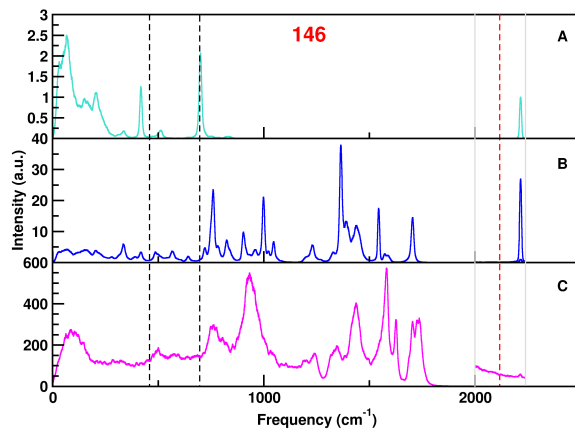
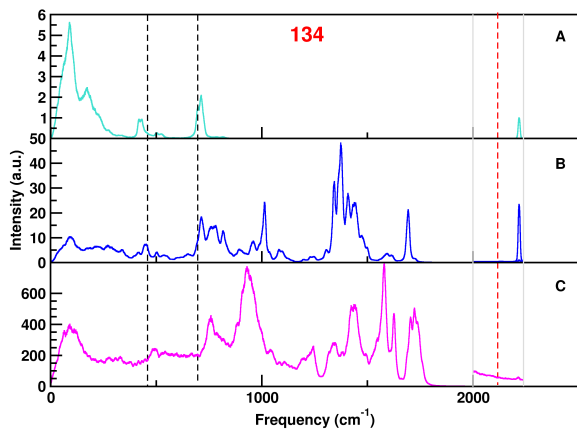
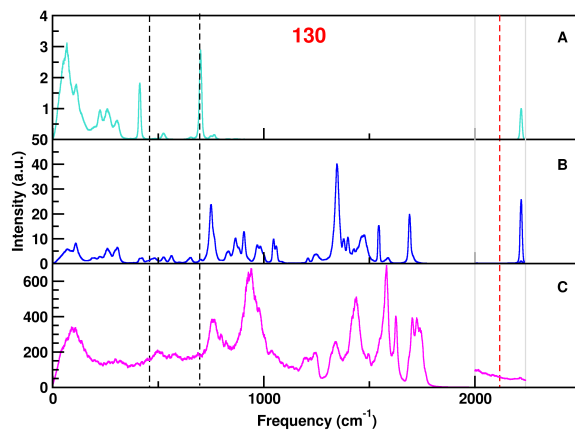
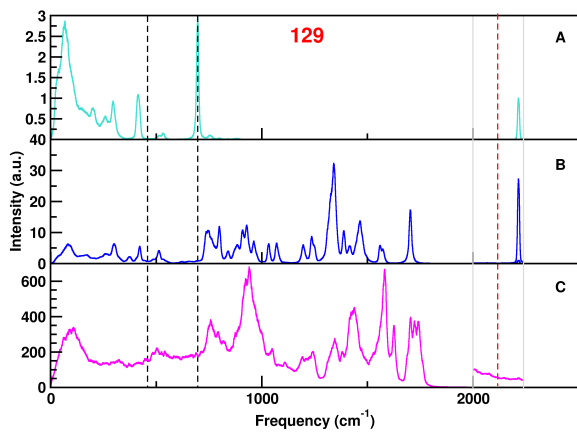
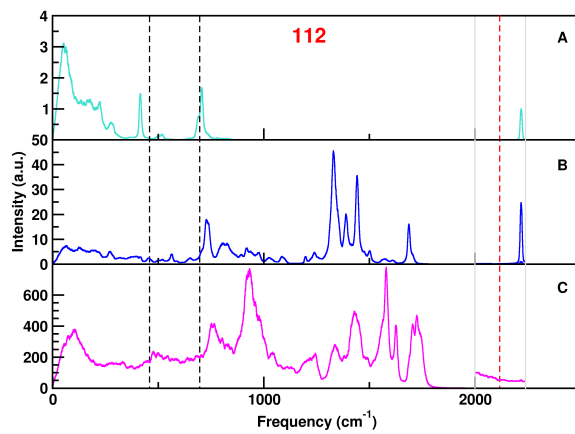
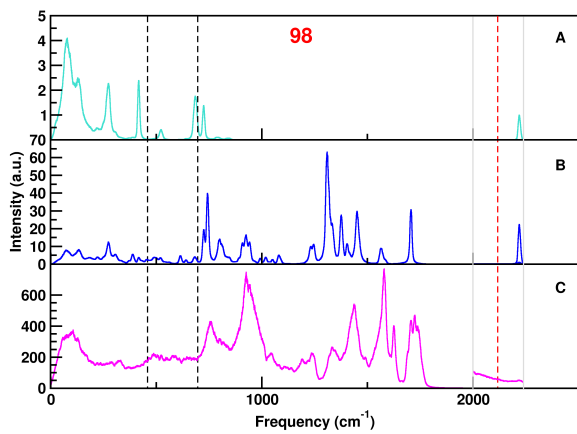
## Data Availability Statement

The data that support the findings of this study are available from the corresponding author upon reasonable request.

## Supporting Information: SCN as a Local Probe of Structural Dynamics









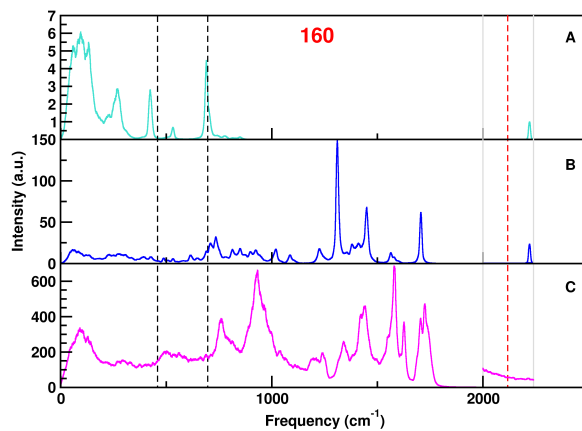


Figure S1: IR spectra of SCN label (a), labelled alanine residue (b), and full lysozyme (c) for all 16 SCN-attached alanine residues in lysozyme. The dashed lines denote the specific peaks of SCN label MeSCN at 459, 697, and 2118 cm<sup>-1</sup>. The range highlighted with grey lines between 2000 and 2240 cm<sup>-1</sup> is rescaled.

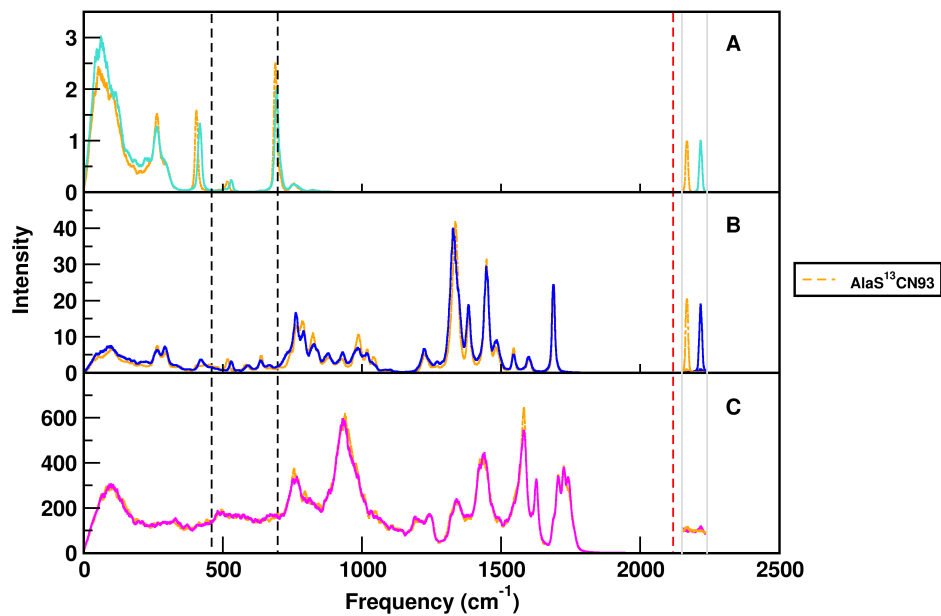


Figure S2: IR spectra of SCN label and isotopically  $S^{13}CN$  label (a), labelled alanine residue and isotopically  $S^{13}CN$  labelled alanine residue (b), and full lysozyme and isotopically  $S^{13}CN$  labelled lysozyme (c) for Ala93SCN. The orange dashed line in each panel represents IR spectra containing isotopically  $S^{13}CN$  label. The dashed lines denote the specific peaks of SCN label MeSCN at 459, 697, and 2118  $cm^{-1}$ . The range illustrated with grey lines between 2150 and 2240  $cm^{-1}$  is rescaled.

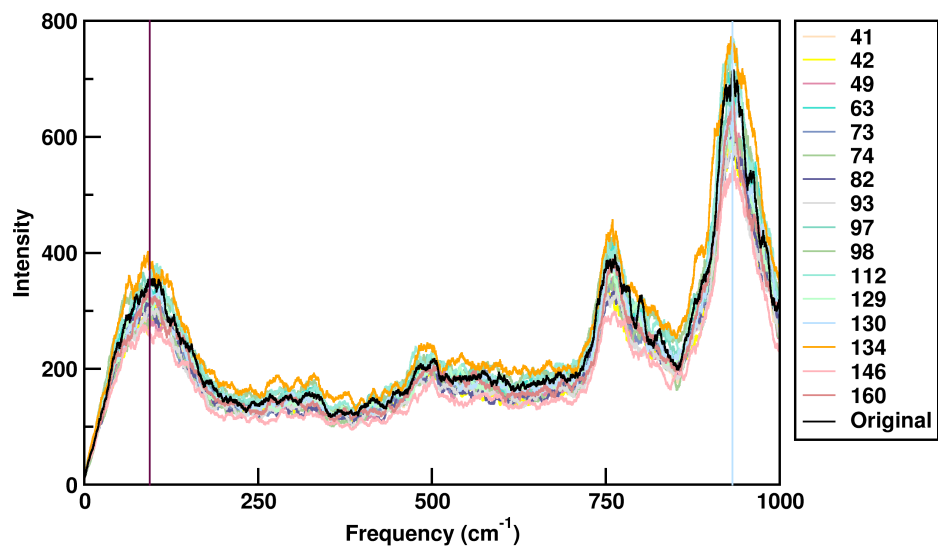


Figure S3: IR spectra of lysozyme for all 16 AlaQQSCN residues with original lysozyme at low frequency.

## References

- (1) Plitzko, J. M.; Schuler, B.; Selenko, P. Structural Biology outside the box - inside the cell. *Curr. Op. Struct. Biol.* **2017**, *46*, 110–121.
- (2) Lane, T. J. Protein structure prediction has reached the single-structure frontier. *Nature Methods* **2023**, *20*, 170–173.
- (3) Yang, H.; Yang, S.; Kong, J.; Dong, A.; Yu, S. Obtaining information about protein secondary structures in aqueous solution using Fourier transform IR spectroscopy. *Nat. Protoc.* **2015**, *10*, 382–396.
- (4) Thielges, M. C.; Fayer, M. D. Protein Dynamics Studied with Ultrafast Two-Dimensional Infrared Vibrational Echo Spectroscopy. *Acc. Chem. Res.* **2012**, *45*, 1866–1874.
- (5) Huang, C.-Y.; Getahun, Z.; Wang, T.; DeGrado, W. F.; Gai, F. Time-Resolved Infrared Study of the Helix-Coil Transition Using <sup>13</sup>C-Labeled Helical Peptides. *J. Am. Chem. Soc.* **2001**, *123*, 12111–12112.
- (6) Taskent-Sezgin, H.; Chung, J.; Banerjee, P. S.; Nagarajan, S.; Dyer, R. B.; Carrico, I.; Raleigh, D. P. Azidohomoalanine: A Conformationally Sensitive IR Probe of Protein Folding, Protein Structure, and Electrostatics. *Angew. Chem. Int. Ed.* **2010**, *49*, 7473–7475.
- (7) Koner, D.; Salehi, S. M.; Mondal, P.; Meuwly, M. Non-conventional force fields for applications in spectroscopy and chemical reaction dynamics. *J. Chem. Phys.* **2020**, *153*, 010901.
- (8) Helbing, J.; Hamm, P. Versatile femtosecond laser synchronization for multiple-timescale transient infrared spectroscopy. *J. Phys. Chem. A* **2023**, *127*, 6347–6356.
- (9) Xie, J.; Schultz, P. G. A chemical toolkit for proteins—an expanded genetic code. *Nat. Rev. Mol. Cell Biol.* **2006**, *7*, 775–782.

- (10) Ma, J.; Pazos, I. M.; Zhang, W.; Culik, R. M.; Gai, F. Site-Specific Infrared Probes of Proteins. *Annu. Rev. Phys. Chem.* **2015**, *66*, 357–377.
- (11) Kim, H.; Cho, M. Infrared Probes for Studying the Structure and Dynamics of Biomolecules. *Chem. Rev.* **2013**, *113*, 5817–5847.
- (12) Zimmermann, J.; Gundogdu, K.; Cremeens, M. E.; Bandaria, J. N.; Hwang, G. T.; Thielges, M. C.; Cheatum, C. M.; Romesberg, F. E. Efforts toward Developing Probes of Protein Dynamics: Vibrational Dephasing and Relaxation of Carbon–Deuterium Stretching Modes in Deuterated Leucine. *J. Phys. Chem. B* **2009**, *113*, 7991–7994.
- (13) King, J. T.; Arthur, E. J.; Brooks, C. L. I.; Kubarych, K. J. Site-Specific Hydration Dynamics of Globular Proteins and the Role of Constrained Water in Solvent Exchange with Amphiphilic Cosolvents. *J. Phys. Chem. B* **2012**, *116*, 5604–5611.
- (14) Tadesse, L.; Nazarbaghi, R.; Walters, L. Isotopically enhanced infrared spectroscopy: a novel method for examining secondary structure at specific sites in conformationally heterogeneous peptides. *J. Am. Chem. Soc.* **1991**, *113*, 7036–7037.
- (15) Salehi, S. M.; Meuwly, M. Site-selective dynamics of azidolysosome. *JCP* **2021**, *154*.
- (16) Edelstein, L.; Stetz, M. A.; McMahan, H. A.; Londergan, C. H. The effects of  $\alpha$ -helical structure and cyanylated cysteine on each other. *J. Phys. Chem. B* **2010**, *114*, 4931–4936.
- (17) McMahan, H. A.; Alfieri, K. N.; Clark, C. A. A.; Londergan, C. H. Cyanylated Cysteine: A Covalently Attached Vibrational Probe of Protein-Lipid Contacts. *J. Phys. Chem. Lett.* **2010**, *1*, 850–855.
- (18) Bischak, C. G.; Longhi, S.; Snead, D. M.; Costanzo, S.; Terrer, E.; Londergan, C. H. Probing Structural Transitions in the Intrinsically Disordered C-Terminal Domain of

- the Measles Virus Nucleoprotein by Vibrational Spectroscopy of Cyanylated Cysteines. *Biophys. J.* **2010**, *99*, 1676–1683.
- (19) Fafarman, A. T.; Webb, L. J.; Chuang, J. I.; Boxer, S. G. Site-specific conversion of cysteine thiols into thiocyanate creates an IR probe for electric fields in proteins. *J. Am. Chem. Soc.* **2006**, *128*, 13356–13357.
- (20) Waegle, M. M.; Culik, R. M.; Gai, F. Site-Specific Spectroscopic Reporters of the Local Electric Field, Hydration, Structure, and Dynamics of Biomolecules. *J. Phys. Chem. Lett.* **2011**, *2*, 2598–2609.
- (21) Phelan, P.; Malthouse, J. P. G. <sup>1</sup>H-NMR spectroscopy of  $\beta$ -thiocyanatoalanine. *Biochem. Soc. Trans.* **1996**, *24*, 130S–130S.
- (22) Maienschein-Cline, M. G.; Londergan, C. H. The CN stretching band of aliphatic thiocyanate is sensitive to solvent dynamics and specific solvation. *J. Phys. Chem. A* **2007**, *111*, 10020–10025.
- (23) Schmidt-Engler, J. M.; Blankenburg, L.; Blasiak, B.; van Wilderen, L. J. G. W.; Cho, M.; Bredenbeck, J. Vibrational Lifetime of the SCN Protein Label in H<sub>2</sub>O and D<sub>2</sub>O Reports Site-Specific Solvation and Structure Changes During PYP's Photocycle. *Anal. Chem.* **2020**, *92*, 1024–1032.
- (24) van Wilderen, L. J. G. W.; Kern-Michler, D.; Mueller-Werkmeister, H. M.; Bredenbeck, J. Vibrational dynamics and solvatochromism of the label SCN in various solvents and hemoglobin by time dependent IR and 2D-IR spectroscopy. *Phys. Chem. Chem. Phys.* **2014**, *16*, 19643–19653.
- (25) MacKerell, A. D. J. et al. All-Atom Empirical Potential for Molecular Modeling and Dynamics Studies of Proteins. *J. Phys. Chem. B* **1998**, *102*, 3586–3616.

- (26) Ho, T.-S.; Rabitz, R. A General Method for Constructing Multidimensional Molecular Potential Energy Surfaces from ab Initio Calculations. *J. Chem. Phys.* **1996**, *104*, 2584–2597.
- (27) Unke, O. T.; Meuwly, M. Toolkit for the Construction of Reproducing Kernel-Based Representations of Data: Application to Multidimensional Potential Energy Surfaces. *J. Chem. Inf. Model.* **2017**, *57*, 1923–1931.
- (28) Schwilk, M.; Ma, Q.; Koepl, C.; Werner, H.-J. Scalable Electron Correlation Methods. 3. Efficient and Accurate Parallel Local Coupled Cluster with Pair Natural Orbitals (PNO-LCCSD). *J. Chem. Theo. Comp.* **2017**, *13*, 3650–3675.
- (29) Ma, Q.; Schwilk, M.; Koepl, C.; Werner, H.-J. Scalable Electron Correlation Methods. 4. Parallel Explicitly Correlated Local Coupled Cluster with Pair Natural Orbitals (PNO-LCCSD-F12) (vol 13, pg 4871, 2017). *J. Chem. Theo. Comp.* **2018**, *14*, 6750.
- (30) Dunning, T. H., Jr. Gaussian basis sets for use in correlated molecular calculations. I. The atoms boron through neon and hydrogen. *J. Chem. Phys.* **1989**, *90*, 1007–1023.
- (31) Werner, H.-J. et al. MOLPRO, Version 2012.1, A Package of ab Initio Programs. 2012.
- (32) Lee, T. J.; Taylor, P. R. A diagnostic for determining the quality of single-reference electron correlation methods. *Int. J. Quant. Chem.* **1989**, *36*, 199–207.
- (33) MacKerell, A. D. et al. All-atom Empirical Potential for Molecular Modeling and Dynamics Studies of Proteins. *J. Phys. Chem. B* **1998**, *102*, 3586–3616.
- (34) Morton, A.; Matthews, B. W. Specificity of ligand binding in a buried nonpolar cavity of T4 lysozyme: linkage of dynamics and structural plasticity. *Biochem.* **1995**, *34*, 8576–8588.
- (35) Salehi, S. M.; Koner, D.; Meuwly, M. Vibrational Spectroscopy of  $\text{N}_3^-$  in the Gas and Condensed Phase. *J. Phys. Chem. B* **2019**, *123*, 3282–3290.

- (36) Gunsteren, W. V.; Berendsen, H. Algorithms for Macromolecular Dynamics and Constraint Dynamics. *Mol. Phys.* **1997**, *34*, 1311–1327.
- (37) Steinbach, P. J.; Brooks, B. R. New Spherical-Cutoff Methods for Long-Range Forces in Macromolecular Simulation. *J. Comput. Chem.* **1994**, *15*, 667–683.
- (38) Ramírez, R.; López-Ciudad, T.; Kumar P, P.; Marx, D. Quantum corrections to classical time-correlation functions: Hydrogen bonding and anharmonic floppy modes. *J. Chem. Phys.* **2004**, *121*, 3973–3983.
- (39) Salehi, S. M.; Koner, D.; Meuwly, M. Dynamics and Infrared Spectroscopy of Monomeric and Dimeric Wild Type and Mutant Insulin. *J. Phys. Chem. B* **2020**, *in print*, in print.
- (40) Moller, K.; Rey, R.; Hynes, J. Hydrogen Bond Dynamics in Water and Ultrafast Infrared Spectroscopy: A Theoretical Study. *J. Phys. Chem. A* **2004**, *108*, 1275–1289.
- (41) Virtanen, P. et al. SciPy 1.0: Fundamental Algorithms for Scientific Computing in Python. *Nat. Methods* **2020**, *17*, 261–272.
- (42) Li, S.; Schmidt, J. R.; Piryatinski, A.; Lawrence, C. P.; Skinner, J. L. Vibrational Spectral Diffusion of Azide in Water. *J. Phys. Chem. B* **2006**, *110*, 18933–18938.
- (43) Lee, M. W.; Carr, J. K.; Göllner, M.; Hamm, P.; Meuwly, M. 2D IR Spectra of Cyanide in Water Investigated by Molecular Dynamics Simulations. *J. Chem. Phys.* **2013**, *139*, 054506.
- (44) Cazade, P.-A.; Bereau, T.; Meuwly, M. Computational Two-Dimensional Infrared Spectroscopy without Maps: N-Methylacetamide in Water. *J. Phys. Chem. B* **2014**, *118*, 8135–8147.
- (45) Shin, S.; Willard, A. P. Characterizing Hydration Properties Based on the Orientational Structure of Interfacial Water Molecules. *J. Chem. Theo. Comp.* **2018**, *14*, 461–465.



- (46) Shin, S.; Willard, A. P. Water's Interfacial Hydrogen Bonding Structure Reveals the Effective Strength of Surface-Water Interactions. *J. Phys. Chem. B* **2018**, *122*, 6781–6789.
- (47) Pezzella, M.; El Hage, K.; Niesen, M. J.; Shin, S.; Willard, A. P.; Meuwly, M.; Karplus, M. Water dynamics around proteins: T-and R-States of hemoglobin and melittin. *J. Phys. Chem. B* **2020**, *124*, 6540–6554.
- (48) Han, J.; Blackburn, N. J.; Loehr, T. M. Identification of the cyanide stretching frequency in the cyano derivative of copper/zinc-superoxide dismutase by IR and Raman spectroscopy. *Inorg. Chem.* **1992**, *31*, 3223–3229.
- (49) Balakhnina, I. A.; Brandt, N. N.; Chikishev, A. Y.; Mankova, A. A.; Shpachenko, I. G. Low-frequency vibrational spectroscopy of proteins with different secondary structures. *J. Biomed. Opt.* **2017**, *22*, 091509.
- (50) El Khoury, Y.; Hellwig, P. Far infrared spectroscopy of hydrogen bonding collective motions in complex molecular systems. *Chem. Comm.* **2017**, *53*, 8389–8399.
- (51) Ding, T.; Middelberg, A. P.; Huber, T.; Falconer, R. J. Far-infrared spectroscopy analysis of linear and cyclic peptides, and lysozyme. *Vib. Spec.* **2012**, *61*, 144–150.
- (52) Buontempo, U.; Careri, G.; Fasella, P.; Ferraro, A. Far-infrared spectra of some globular proteins. *Biopol.: Orig. Res. Biomol.* **1971**, *10*, 2377–2386.
- (53) Humphrey, W.; Dalke, A.; Schulten, K. VMD – Visual Molecular Dynamics. *Journal of Molecular Graphics* **1996**, *14*, 33–38.
- (54) Pagano, P.; Guo, Q.; Kohen, A.; Cheatum, C. M. Oscillatory enzyme dynamics revealed by two-dimensional infrared spectroscopy. *J. Phys. Chem. Lett.* **2016**, *7*, 2507–2511.
- (55) Chung, J. K.; Thielges, M. C.; Fayer, M. D. Dynamics of Folded and Unfolded Villin

- Headpiece (HP35) Measured with Ultrafast 2DIR Vibrational Echo Spectroscopy. *Proc. Natl. Acad. Sci.* **2011**, *108*, 3578–3583.
- (56) Bagchi, S.; Boxer, S. G.; Fayer, M. D. Ribonuclease S Dynamics Measured Using a Nitrile Label with 2D IR Vibrational Echo Spectroscopy. *J. Phys. Chem. B* **2012**, *116*, 4034–4042.
- (57) Bloem, R.; Koziol, K.; Waldauer, S. A.; Buchli, B.; Walser, R.; Samatanga, B.; Jele-sarov, I.; Hamm, P. Ligand Binding Studied by 2DIR Spectroscopy Using the Azidohomoalanine Label. *J. Phys. Chem. B* **2012**, *116*, 13705–13712.
- (58) Mondal, P.; Meuwly, M. Vibrational Stark Spectroscopy for Assessing Ligand-Binding Strengths in a Protein. *Phys. Chem. Chem. Phys.* **2017**, *19*, 16131–16143.
- (59) Levinson, N. M.; Boxer, S. G. A conserved water-mediated hydrogen bond network defines bosutinib’s kinase selectivity. *Nat. Chem. Biol.* **2014**, *10*, 127–132.
- (60) Layfield, J. P.; Hammes-Schiffer, S. Calculation of Vibrational Shifts of Nitrile Probes in the Active Site of Ketosteroid Isomerase upon Ligand Binding. *J. Am. Chem. Soc.* **2013**, *135*, 717–725.
- (61) Kuroda, D. G.; Bauman, J. D.; Challa, J. R.; Patel, D.; Troxler, T.; Das, K.; Arnold, E.; Hochstrasser, R. M. Snapshot of the equilibrium dynamics of a drug bound to HIV-1 reverse transcriptase. *Nat. Chem.* **2013**, *5*, 174–181.
- (62) Liu, J.; Strzalka, J.; Tronin, A.; Johansson, J. S.; Blasie, J. K. Mechanism of Interaction between the General Anesthetic Halothane and a Model Ion Channel Protein, II: Fluorescence and Vibrational Spectroscopy Using a Cyanophenylalanine Probe. *Biophys. J.* **2009**, *96*, 4176–4187.
- (63) Lee, G.; Kossowska, D.; Lim, J.; Kim, S.; Han, H.; Kwak, K.; Cho, M. Cyanamide as

- an Infrared Reporter: Comparison of Vibrational Properties between Nitriles Bonded to N and C Atoms. *J. Phys. Chem. B* **2018**, *122*, 4035–4044.
- (64) Kozinski, M.; Garrett-Roe, S.; Hamm, P. 2D-IR spectroscopy of the sulfhydryl band of cysteines in the hydrophobic core of proteins. *J. Phys. Chem. B* **2008**, *112*, 7645–7650.
- (65) Zimmermann, J.; Thielges, M. C.; Yu, W.; Dawson, P. E.; Romesberg, F. E. Carbon-Deuterium Bonds as Site-Specific and Nonperturbative Probes for Time-Resolved Studies of Protein Dynamics and Folding. *J. Phys. Chem. Lett.* **2011**, *2*, 412–416.
- (66) King, J. T.; Kubarych, K. J. Site-specific coupling of hydration water and protein flexibility studied in solution with ultrafast 2D-IR spectroscopy. *J. Am. Chem. Soc.* **2012**, *134*, 18705–18712.
- (67) King, J. T.; Arthur, E. J.; Brooks III, C. L.; Kubarych, K. J. Site-specific hydration dynamics of globular proteins and the role of constrained water in solvent exchange with amphiphilic cosolvents. *J. Phys. Chem. B* **2012**, *116*, 5604–5611.
- (68) King, J. T.; Arthur, E. J.; Brooks, C. L., III; Kubarych, K. J. Crowding Induced Collective Hydration of Biological Macromolecules over Extended Distances. *J. Am. Chem. Soc.* **2014**, *136*, 188–194.
- (69) Ramos, S.; Horness, R. E.; Collins, J. A.; Haak, D.; Thielges, M. C. Site-specific 2D IR spectroscopy: a general approach for the characterization of protein dynamics with high spatial and temporal resolution. *Phys. Chem. Chem. Phys.* **2019**, *21*, 780–788.
- (70) Bloem, R.; Koziol, K.; Waldauer, S. A.; Buchli, B.; Walser, R.; Samatanga, B.; Jellesarov, I.; Hamm, P. Ligand Binding Studied by 2D IR Spectroscopy Using the Azidohomoalanine Label. *J. Phys. Chem. B* **2012**, *116*, 13705–13712.
- (71) Kramer, C.; Geddeck, P.; Meuwly, M. Atomic Multipoles: Electrostatic Potential Fit,

- Local Reference Axis Systems and Conformational Dependence. *J. Comp. Chem.* **2012**, *33*, 1673–1688.
- (72) Bereau, T.; Kramer, C.; Meuwly, M. Leveraging Symmetries of Static Atomic Multipole Electrostatics in Molecular Dynamics Simulations. *J. Chem. Theo. Comp.* **2013**, *9*, 5450–5459.
- (73) Devereux, M.; Raghunathan, S.; Fedorov, D. G.; Meuwly, M. A novel, computationally efficient multipolar model employing distributed charges for molecular dynamics simulations. *J. Chem. Theo. Comp.* **2014**, *10*, 4229–4241.
- (74) Unke, O. T.; Devereux, M.; Meuwly, M. Minimal distributed charges: Multipolar quality at the cost of point charge electrostatics. *J. Chem. Phys.* **2017**, *147*, 161712.
- (75) Shirley, J. C.; Baiz, C. R. Experimental two-dimensional infrared spectra of methyl thiocyanate in water and organic solvents. *J. Chem. Phys.* **2024**, *160*.
- (76) Zhao, R.; Shirley, J. C.; Lee, E.; Grofe, A.; Li, H.; Baiz, C. R.; Gao, J. Origin of thiocyanate spectral shifts in water and organic solvents. *J. Chem. Phys.* **2022**, *156*.
- (77) Oh, K.-I.; Choi, J.-H.; Lee, J.-H.; Han, J.-B.; Lee, H.; Cho, M. Nitrile and thiocyanate IR probes: Molecular dynamics simulation studies. *J. Chem. Phys.* **2008**, *128*.
- (78) Bereau, T.; Kramer, C.; Meuwly, M. Leveraging Symmetries of Static Atomic Multipole Electrostatics in Molecular Dynamics Simulations. *J. Chem. Theo. Comp.* **2013**, *9*, 5450–5459.
- (79) Turan, H. T.; Meuwly, M. Spectroscopy, Dynamics, and Hydration of S-Nitrosylated Myoglobin. *J. Phys. Chem. B* **2021**, *in print*.
- (80) Turan, H. T.; Meuwly, M. Local Hydration Control and Functional Implications Through S-Nitrosylation of Proteins: Kirsten Rat Sarcoma Virus (K-RAS) and Hemoglobin (Hb). *J. Phys. Chem. B* **2023**, *127*, 1526–1539.

- (81) Suydam, I. T.; Snow, C. D.; Pande, V. S.; Boxer, S. G. Electric Fields at the Active Site of an Enzyme : Direct Comparison of Experiment with Theory. *Science* **2006**, *313*, 200–204.